Lateral migration of a viscoelastic drop in a Newtonian fluid in a shear flow near a wall

Swarnajay Mukherjee and Kausik Sarkar

Citation: Physics of Fluids (1994-present) **26**, 103102 (2014); doi: 10.1063/1.4897921
View online: http://dx.doi.org/10.1063/1.4897921
View Table of Contents: http://scitation.aip.org/content/aip/journal/pof2/26/10?ver=pdfcov
Published by the AIP Publishing

PHYSICS OF FLUIDS **26**, 103102 (2014)

Lateral migration of a viscoelastic drop in a Newtonian fluid in a shear flow near a wall

Swarnajay Mukherjee[1,a)] and Kausik Sarkar[1,2]
[1]*Department of Mechanical Engineering, University of Delaware, Newark, Delaware 19716-3140, USA*
[2]*Department of Mechanical and Aerospace Engineering, George Washington University, Washington, DC 20052, USA*

(Received 4 June 2014; accepted 12 September 2014; published online 22 October 2014)

Wall induced lateral migration of a viscoelastic (FENE-MCR) drop in a Newtonian fluid is investigated. Just like a Newtonian drop, a viscoelastic drop reaches a quasi-steady state where the lateral velocity only depends on the instantaneous distance from the wall. The drop migration velocity and the deformation scale inversely with the square and the cube of the distance from the wall, respectively. The migration velocity varies non-monotonically with increasing viscoelasticity (increasing Deborah number); initially increasing and then decreasing. An analytical explanation has been given of the effects by computing the migration velocity as arising from an image stresslet field due to the drop. The semi-analytical expression matches well with the simulated migration velocity away from the wall. It contains a viscoelastic stresslet component apart from those arising from interfacial tension and viscosity ratio. The migration dynamics is a result of the competition between the viscous (interfacial tension and viscosity ratio) and the viscoelastic effects. The viscoelastic stresslet contribution towards the migration velocity steadily increases. But the interfacial stresslet—arising purely from the drop shape—first increases and then decreases with rising Deborah number causing the migration velocity to be non-monotonic. The geometric effect of the interfacial stresslet is caused by a corresponding nonmonotonic variation of the drop inclination. High viscosity ratio is briefly considered to show that the drop viscoelasticity could stabilize a drop against breakup, and the increase in migration velocity due to viscoelasticity is larger compared to the viscosity-matched case. © *2014 AIP Publishing LLC*. [http://dx.doi.org/10.1063/1.4897921]

I. INTRODUCTION

Cross-stream migration of drops and particles plays a crucial role in flows of industrial emulsions—oil production,[1] food processing,[2] injection molding of plastics with fillers[3,4]—as well as in biological flows of cells in small capillaries[5] and microfluidic devices.[6] In Stokes flow, a neutrally buoyant rigid particle in a viscous liquid does not migrate across streamlines in a wall bounded shear due to symmetry under flow reversal.[7–9] Reversibility can be broken by particle deformability, viscoelasticity, or inertia. In this paper, we numerically investigate a viscoelastic drop migrating under shear near a wall in a viscous liquid, and provide an analytic explanation of the phenomenon.

Drop migration in Newtonian systems has been studied extensively using experimental,[10–17] theoretical,[18–26] and numerical techniques,[27–29] and excellent reviews have been written.[30,31] In contrast, the literature of migration in non-Newtonian systems[32–40] is meager, and most of it describes migration of rigid particles.[41–44] Apart from experimental observations,[10,11,33,40] there has been only one report[45] of theoretical investigation of viscoelastic effects on drop migration, where the authors performed a rigorous perturbative analysis of the viscoelastic effects of both drop and matrix

[a)]Present address: Schlumberger Rosharon Technology Center, Rosharon, Texas 77583-1590, USA.

phases on migration using a second order fluid model. To our knowledge, there was no numerical investigation of drop migration in a viscoelastic system before our recent investigation of a viscous drop migrating in a FENE matrix in shear near a wall—N/V (Newtonian in viscoelastic).[46] Readers are referred there for a detailed discussion of the migration literature. The migration is caused by a stresslet field induced by the drop in presence of the wall.[12] The matrix viscoelasticity retards drop migration, an effect we clearly show to arise from a non-Newtonian contribution to the stresslet field. It is computed as an integral of the normal stress differences in the flow field. Here, we extend the numerical and theoretical analysis to the V/N case—a viscoelastic drop in a Newtonian fluid.

Note that the perturbative analysis[45] predicted that viscoelasticity either in drop or matrix phase promotes drop migration in plane shear, in contradiction to recent experimental and numerical findings in the literature which show rigid particles in a sheared viscoelastic medium moving closer to a wall.[47] In the limit of a high viscosity, a viscous drop behaves similar to a rigid particle. Such contradiction points to the limitation of perturbative analysis and demonstrates a need for full scale numerical simulation. Such simulations, especially in simple canonical systems—e.g., involving one drop in shear,[48–52] extension,[53] or gravitational fall[54] using simplest possible constitutive equations[48–54]—are critical for developing physical intuition about viscoelastic effects in multiphase systems. Unlike viscous systems, our understanding of viscoelasticity is severely limited, and yet of great importance for flow modeling and simulation. The difficulty lies in the subtle competition between multiple effects in viscoelastic system often giving rise to baffling experimental observations. For instance, there were contradictory observations about effects of matrix viscoelasticity on drop deformation in the literature.[55–57] Numerical simulation showed that it can both decrease drop migration at small Deborah or Wissenberg numbers by aligning a drop away from the axis of extension, or increase at higher Deborah numbers by local stretching at the drop tips.[49,57] The effects of viscoelasticity in the drop phase is typically smaller than those due to matrix viscoelasticity. However, they also generate several interesting phenomena. Although a viscoelastic drop deforms less in shear compared to a viscous drop due to normal stresses in the circular streamlines,[48] at higher viscosity ratios, viscoelastic drop deformation can be greater than the viscous case. The phenomenon arises due to a reduction of strain rate at higher viscosity ratios resulting in a reduction in deformation-inhibiting normal stresses, and simultaneous alignment with extension axis that enhances deformation.

Here, we have used a front tracking finite difference method[58] with a modified version of the finitely extensible nonlinear elastic model due to Chilcott and Rallison (FENE-MCR).[59] The FENE-MCR model has a single relaxation time, a constant shear viscosity and a positive first normal stress difference—all characteristics of a Boger fluid—and has been used in many viscoelastic studies.[60–65] The mathematical formulation and its numerical implementation are described in Sec. II. Section III discusses the problem setup and convergence. Section IV presents and analyzes the results of the simulation. A theoretical analysis relating the interfacial, viscous, and viscoelastic stresses in the system with the lateral migration velocity is presented following the numerical investigation. Section V summarizes the findings.

II. MATHEMATICAL FORMULATION AND NUMERICAL IMPLEMENTATION

The mathematical formulation and the numerical implementation for Newtonian drops migrating in a viscoelastic shear flow have been described in our recent publication[46] and the formulation here is similar. Therefore, it is only briefly sketched for completeness. The velocity field $\mathbf{u}$ of the droplet matrix system is governed by the incompressible momentum conservation equations

$$\begin{aligned} &\frac{\partial(\rho\mathbf{u})}{\partial t} + \nabla\cdot(\rho\mathbf{u}\mathbf{u}) = \nabla\cdot\boldsymbol{\tau} - \int_{\partial\mathrm{B}} d\mathbf{x_B}\kappa\mathbf{n}\Gamma\delta(\mathbf{x}-\mathbf{x_B}),\\ &\nabla\cdot\mathbf{u} = \mathbf{0}, \end{aligned} \tag{1}$$

in the entire domain Ω. The total stress $\boldsymbol{\tau}$ is decomposed into pressure, polymeric and viscous parts:

$$\boldsymbol{\tau} = -p\mathbf{I} + \mathbf{T}^p + \mathbf{T}^v, \quad \mathbf{T}^v = \mu_s\mathbf{D}, \tag{2}$$

where p is the pressure, μ_s is the solvent viscosity, and $\mathbf{D} = (\nabla\mathbf{u}) + (\nabla\mathbf{u})^T$ is the deformation rate tensor. The superscript T represents the transpose. $\mathbf{T}^p$ is the extra stress (or viscoelastic stress) due to the presence of polymer. Γ is the interfacial tension (constant), ∂B represents the surface of the drop consisting of points $\mathbf{x}_B$, κ is the local curvature, $\mathbf{n}$ is the outward normal, and $\delta(\mathbf{x} - \mathbf{x}_B)$ is the three dimensional Dirac delta function. The viscoelastic stress $\mathbf{T}^p$ is computed through the conformation tensor $\mathbf{A}$ which satisfies the following equation:

$$\frac{\partial \mathbf{A}}{\partial t} + \mathbf{u}\cdot\nabla\mathbf{A} = \nabla\mathbf{u}\cdot\mathbf{A} + \mathbf{A}\cdot(\nabla\mathbf{u})^T - \frac{f}{\lambda}(\mathbf{A} - \mathbf{I}), \tag{3}$$

where $f = \frac{L^2}{L^2 - tr(\mathbf{A})}$, μ_p is the polymeric viscosity, λ is the relaxation time, and L is the finite extensibility.

The relation between the stress $\mathbf{T}^p$ and conformation tensor $\mathbf{A}$ is

$$\mathbf{A} = \left(\frac{\lambda}{\mu_p f}\right)\mathbf{T}^p + \mathbf{I}. \tag{4}$$

Therefore, the constitutive equation for the stresses becomes

$$\begin{aligned} &\frac{\partial \mathbf{T}^p}{\partial t} + \left\{\mathbf{u}\cdot\nabla\mathbf{T}^p - \nabla\mathbf{u}\cdot\mathbf{T}^p - \mathbf{T}^p\cdot\nabla\mathbf{u}^T\right\} + \\ &f\,\mathbf{T}^p\left[\frac{\partial}{\partial t}(1/f) + \mathbf{u}\cdot\nabla(1/f)\right] + \frac{f}{\lambda}\mathbf{T}^p = \frac{f}{\lambda}\mu_p\mathbf{D}, \end{aligned} \tag{5}$$

$$f = \frac{L^2 + \lambda/\mu_p\left(\sum T^p_{ii}\right)}{L^2 - 3}.$$

In the limit of $L \to \infty$, we obtain the Oldroyd-B equation. The terms $f\mathbf{T}^p\left[\frac{\partial}{\partial t}(1/f) + \mathbf{u}\cdot\nabla(1/f)\right]$ are negligible in our simulations, and by dropping them we arrive at the FENE-MCR equation:

$$\frac{\partial \mathbf{T}^p}{\partial t} + \left\{\mathbf{u}\cdot\nabla\mathbf{T}^p - \nabla\mathbf{u}\cdot\mathbf{T}^p - \mathbf{T}^p\cdot\nabla\mathbf{u}^T\right\} + \frac{f}{\lambda}\mathbf{T}^p = \frac{f}{\lambda}\mu_p\mathbf{D}. \tag{6}$$

Using the elastic and viscous stress splitting method proposed and developed by us,[53] the viscoelastic stress for FENE-MCR equation is given by

$$\begin{aligned} \left(\mathbf{T}^p\right)^{n+1} = &\left[\left(\mathbf{T}^p\right)^n - \left(\mu_p\mathbf{D}\right)^n\right]e^{-(f/\lambda)\Delta t} + \left(\mu_p\mathbf{D}\right)^n \\ &- \frac{\lambda}{f}\left[\mathbf{u}\cdot\nabla\mathbf{T}^p - \nabla\mathbf{u}\cdot\mathbf{T}^p - \mathbf{T}^p\cdot\nabla\mathbf{u}^T\right]^n\left[1 - e^{-(f/\lambda)\Delta t}\right]. \end{aligned} \tag{7}$$

Note that Eq. (7) appeared in our recent article[46] with a slight typographical error. A front-tracking finite difference method is used to simulate the drop dynamics.

III. PROBLEM SETUP AND CONVERGENCE

As in our previous study,[46] the problem is started by placing a spherical drop of radius a in a three dimensional rectangular computational domain at $t = 0$ at a distance h_i from the bottom wall of the domain. The domain is periodic in the flow (x) and the vorticity (z) directions with domain sizes in those directions $L_x = 10a$ and $L_z = 5a$, respectively. The size (L_y) in the gradient direction (y) is $10a$ with walls at the top and the bottom boundary. The lower wall is stationary and the upper wall is impulsively started at $t = 0$ with velocity U creating a shear rate of $\dot{\gamma} = U/L_y$. Other details of the problem setup can be found in our previous publication.[46] Nondimensionalizing the problem using a and $\dot{\gamma}^{-1}$ we obtain the non-dimensional parameters Reynolds number $\mathrm{Re} = \rho_m a^2\dot{\gamma}/\mu_m$, capillary number $Ca = \mu_m a\dot{\gamma}/\Gamma$, Deborah number $De = \lambda\dot{\gamma}$, viscosity ratio $\lambda_\mu = \mu_d/\mu_m$, density ratio $\lambda_\rho = \rho_d/\rho_m$, and $\beta = \mu_{pd}/\mu_d$—the ratio of the polymeric to the total drop viscosity. The total viscosity of the drop is given as $\mu_d = \mu_{sd} + \mu_{pd}$, sum of the solvent and polymeric viscosities. We have fixed the density ratio at 1 and L at 20. The values of β and viscosity ratio are 0.5 and 1, except where we have studied their effects. The code is explicit which restricts us to a small non-zero

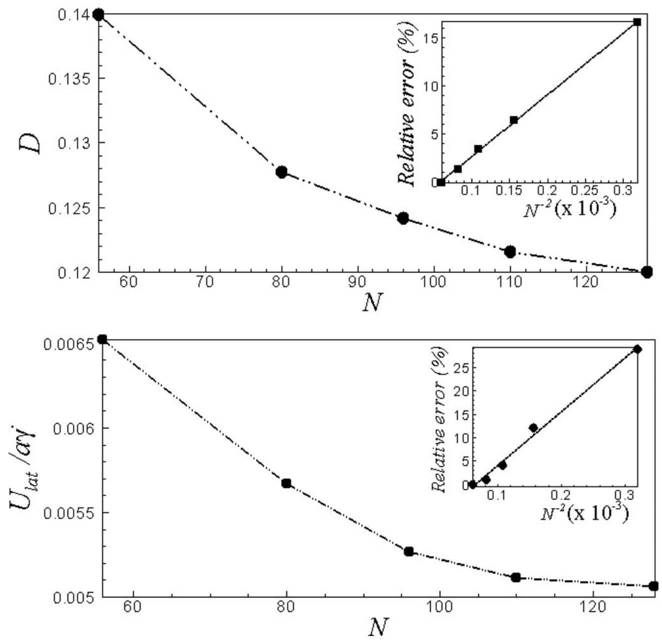

FIG. 1. Quadratic convergence of the viscoelastic algorithm. N is the number of grid points in the x and y directions. Deformation (top) and velocity (bottom) are plotted for several grid discretizations for $De = 1.5$, $Ca = 0.1$ at $h/a = 1.5$.

Reynolds number, for which we have chosen a value of 0.03. In our recent paper,[46] simulation at $\mathrm{Re} = 0.03$ has shown an excellent match with Stokes flow analytical results and boundary element (BEM) simulations.

The convergence of the viscoelastic algorithms (Oldroyd-B and FENE-MCR) has been established in our previous publications[46,48–52,54] for several problems related to drop dynamics. The convergence of drop deformation parameter $D = (L - B)/(L + B)$ (assuming the drop to be an ellipsoid, L and B are the major and the minor axes) and lateral migration velocity is plotted in Fig. 1. N is the number of grid points in the x and y directions; z direction has w $N/2$ grid points. Inset shows the quadratic convergence of the algorithm. We choose $96 \times 96 \times 48$ discretization in the flow, gradient and vorticity directions, respectively, with error in velocity less than 4.5%. The effects of finite domain lengths have been carefully investigated by changing the domain size with minimal effects from the periodic images of the drop in the x and the z directions. We also verified that the effect of the upper wall (at a distance of $L_y = 10a$ from the lower one) has very little effects on the migration velocity for cases considered here (all are restricted to $h < 2.5a$). Note that recent simulations explored effects of domain confinement on particle motion in a viscoelastic medium.[66]

IV. RESULTS

In the Stokes limit, the steady lateral migration $U_{lat}/\dot{\gamma}a$ is known to scale as $\propto Ca(a/h)^2$. The proportionality constant was obtained by various investigators through perturbation analysis as well as BEM simulation—0.6,[45] 0.583,[12] 0.44–0.49,[28] and 0.41.[24] In our recent publication,[46] we showed the same approximate scaling (with constant ∼0.48) for migration velocity, matching very well with the BEM simulation.[28] The deformation of a drop as a function of distance was compared with the theoretical expression of Shapira and Haber.[23] For higher viscosity systems, we compared our results with BEM simulations of Uijttewaal and Nijhof.[27]

A. Effects of Deborah number, β, and capillary number

To study the effects of De and β, we have fixed the capillary number at $Ca = 0.1$. In Fig. 2(a), we plot the migration velocity as a function of instantaneous distance from the wall for several initial drop

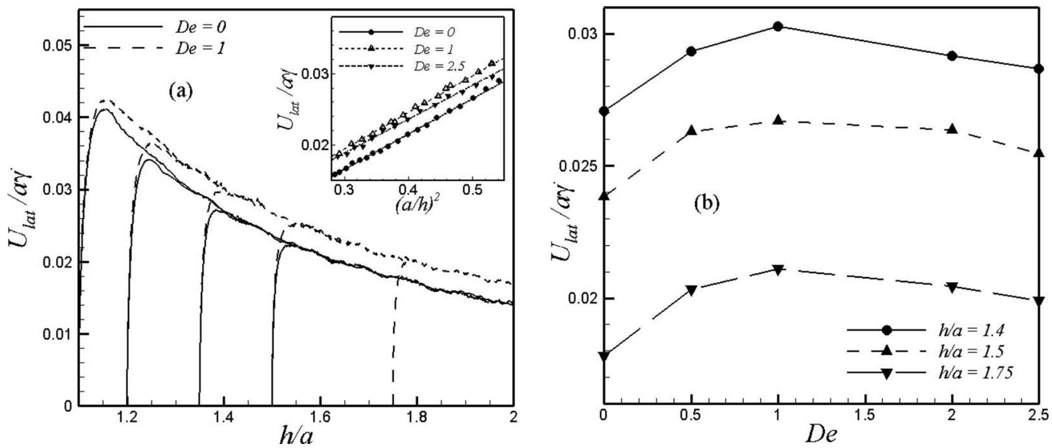

FIG. 2. (a) Lateral migration velocity vs. the distance of the drop from the wall for varying De and initial drop height h_i/a for $Ca = 0.1$. Inset plots quasi-steady migration velocity against inverse square of the instantaneous wall distance for different Deborah numbers. The symbols are data from the simulations and the lines are linear fits. (b) Quasi-steady lateral migration velocity vs. De for different wall-drop distances for $Ca = 0.1$.

positions both for the Newtonian and a viscoelastic ($De = 1$) cases. We notice that a viscoelastic drop migrates quicker and possesses higher velocity than a Newtonian drop. Note that this is in contrast to the case of a viscous drop in a viscoelastic matrix (N/V) where matrix viscoelasticity retards drop migration.[46] Also note that the viscoelastic effects are much less pronounced in this (V/N) case than in the N/V case, as the viscoelasticity here is limited inside the confined space of a drop where the magnitude of shear remains small giving rise to small viscoelastic stresses. In free shear as well, the deviation in drop dynamics in the N/V case deviates only by a small amount from the purely Newtonian (N/N) case.[48,51,67] Similar to the purely Newtonian[28] as well as the N/V system,[46] the viscoelastic drop after a transient period settles in a quasi-steady state of migration where the drop velocity depends only on the instantaneous separation from the wall h independent of the initial separation h_i; curves for different initial positions collapse on a single curve. Here onward, we concentrate on the quasi-steady dynamics until in Subsection III C, where we investigate transient effects for large deformation. The inset of Fig. 2(a) shows the approximate scaling $\sim(a/h)^2$ similar to the N/N and the N/V cases. It also shows that drop viscoelasticity initially increases migration velocity and then decreases at higher De. The non-monotonicity is clearly observed in Fig. 2(b) where we have plotted quasi-steady lateral migration velocities as a function of De for several instantaneous wall to drop distances all for $Ca = 0.1$.

In Fig. 3, we plot the vertical component of the viscoelastic force ($\int_{\partial B}(\mathbf{n} \cdot \mathbf{T}^p)da$) where $\mathbf{n}$ is the outward normal to the drop surface ∂B. Fig. 3(a) plots it vs. the instantaneous distance from the wall for three different initial heights and two Deborah numbers. The force curve for a particular Deborah number is independent of the initial drop height and depends only on the instantaneous position. Fig. 3(b) plotting viscoelastic forces vs. De for three different instantaneous heights shows that the viscoelastic force is nonmonotonic which in turn causes the velocity to be nonmonotonic as seen in Fig. 2(b).

In Fig. 4(a), we plot deformation for varying De. In free shear, with increasing De, the drop deformation decreases.[48] The decrease in deformation in presence of viscoelasticity is due to the presence of inhibiting normal stresses at the tip of the drop.[48] At higher viscosity ratios the deformation is non-monotonic.[51] Shapira and Haber showed that in Stokes flow deformation varies as $D \sim (a/h)^3$.[23] The same scaling is seen in our simulation. Figure 4(b) shows that the inclination angle of the deformed drop increases with De as in the free shear case and it scales as $\sim(a/h)^2$. Inset of Figure 4(b) plots the angle of inclination at $h/a = 1.4$ and 1.75 to show that it varies nonmonotonically with De. We will show that the angle of inclination, a geometric effect, plays critical role in determining the variation of the migration velocity.

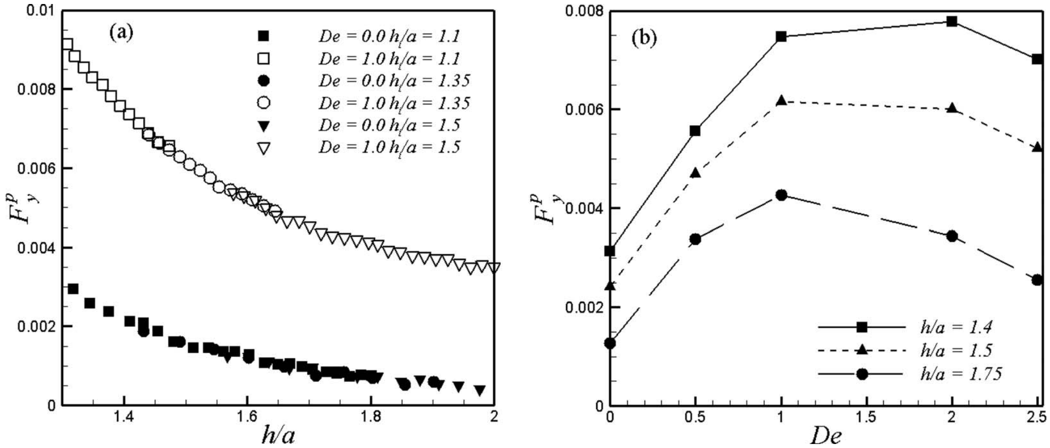

FIG. 3. (a) Quasi-steady viscoelastic force on the drop vs. the distance of the drop from the wall for varying *De* and initial drop height (h_i/a) for $Ca = 0.1$. (b) Quasi-steady viscoelastic net force on the drop vs. *De* for different drop distances.

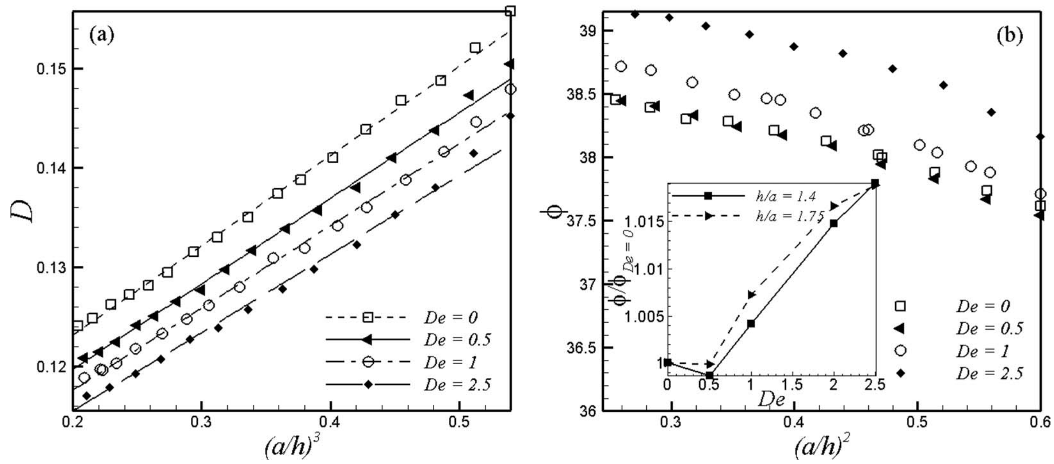

FIG. 4. (a) Quasi-steady deformation vs. the inverse of the cube of the drop-to-wall distance for varying *De* for $Ca = 0.1$. The symbols are data from the simulations and the lines are the linear fits. (b) Inclination angle against $(a/h)^2$ for the same *Ca* and *De*. Inset shows inclination relative to the Newtonian value versus *De* at two drop-wall separations.

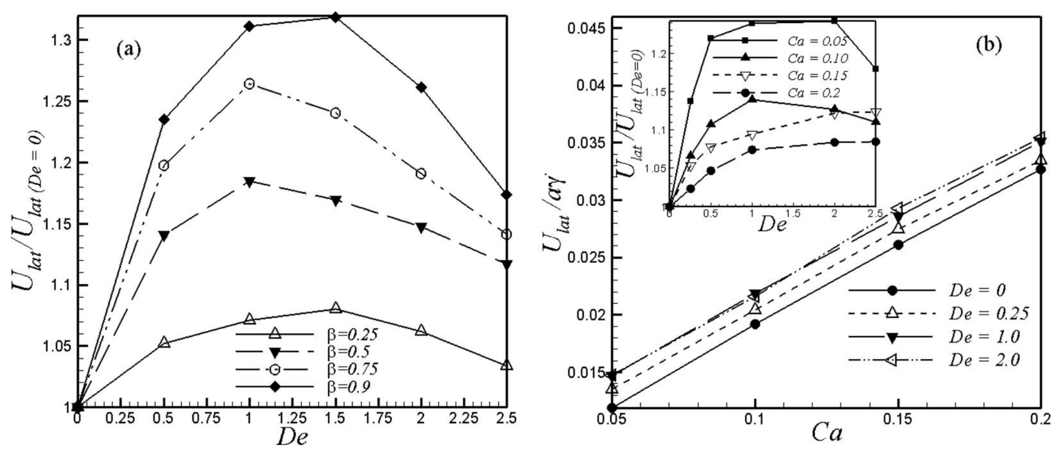

FIG. 5. (a) Lateral migration velocity plotted for varying *De* for different values of β at $h/a = 1.75$. (b) Lateral migration velocity as a function of *Ca* for different Deborah numbers at $h/a = 1.7$. Inset shows the variation of lateral velocities against *De* for several *Ca* when the velocities are normalized by their respective Newtonian value at $h/a = 1.7$.

In Fig. 5(a), we investigate the effects of polymer viscosity in the drop fluid by varying β. The migration velocity as a function of *De* at *h/a* = 1.75 shows that migration velocity increases with increasing β. Fig. 5(b) shows that $U_{lat}/\dot{\gamma}a \propto Ca$ similar to the Newtonian case for different *De* values. By plotting migration velocity normalized by its Newtonian value in the inset, one sees that as *Ca* increases, the viscoelastic effects diminish, as was also seen in N/V case.[46]

B. A far-field theory of viscoelastic drop migration

In our recent paper on the N/V migration case,[46] we developed a far-field theory for drop migration. Note that the only analytical theory available for effects of viscoelasticity on drop migration is due to Chan and Leal,[45] where the authors used a algebraically demanding perturbation analysis to the problem. The analysis although rigorous does not elucidate the underlying physics. The far field theory is based on an earlier idea proposed by Smart and Leighton[12] that the migration arises due to an image stresslet field induced by the drop in presence of the wall. In our previous paper, we further developed the idea extending it to the case of a viscoelastic matrix.[46] We clearly showed that the stresslet had three contributions due to the interfacial tension, viscosity ratio, and matrix viscoelasticity. With increasing viscoelasticity, in a viscosity-matched system, the interfacial contribution increases due to increasing inclination angle. But it is outweighed by the direct reduction in the non-Newtonian part due to matrix viscoelasticity resulting in an overall decrease in migration velocity. We also recently developed the same theoretical analysis for migration of a capsule enclosed by an elastic membrane.[68] Here we apply the technique to the viscoelastic drop case. The derivation is similar to the viscoelastic matrix case but differs in an important way—the argument for the Taylor series expansion of the single and double layer Green's functions are far more straight forward here in V/N case than in the N/V case. Here we only briefly sketch the analysis omitting the details presented previously.[46]

We rewrite the governing equations (the equations used for the front tracking simulation) in the limit of zero Reynolds number as

$$\begin{aligned} &-\nabla p + \mu_m \nabla^2 \mathbf{u} = 0, \\ &-\nabla \tilde{p} + \mu_d \nabla^2 \tilde{\mathbf{u}} = -\nabla \cdot (\tilde{\mathbf{T}}^p - \mu_{pd} \tilde{\mathbf{D}}) = -\nabla \cdot \tilde{\mathbf{T}}^{NN}, \end{aligned} \tag{8}$$

in the matrix and the drop phase, respectively. Variables with a tilde represent field variables inside the drop. The redefined non-Newtonian stress $\tilde{\mathbf{T}}^{NN} = \tilde{\mathbf{T}}^p - \mu_{pd}\tilde{\mathbf{D}}$ gives rise to a force term in the Stokes equation in the drop phase. Following the usual manipulation,[46] one can write the solution outside the drop using a Green's function formulation

$$\begin{aligned} u_j(\mathbf{x}) = u_j^{\infty} - \frac{1}{8\pi\mu_m} \int_{A_d} f_i(\mathbf{y}) G_{ij}(\mathbf{x},\mathbf{y}) dA(\mathbf{y}) + \frac{1}{8\pi} \int_{A_d} u_i(\mathbf{y}) M_{ijk}(\mathbf{x},\mathbf{y}) n_k(\mathbf{y}) dA(\mathbf{y}), \\ G_{ij}(\mathbf{x},\mathbf{y}) = G_{ij}^{FS}(\mathbf{x},\mathbf{y}) + G_{ij}^{w}(\mathbf{x},\mathbf{y}), \quad M_{ijk}(\mathbf{x},\mathbf{y}) = M_{ijk}^{FS}(\mathbf{x},\mathbf{y}) + M_{ijk}^{w}(\mathbf{x},\mathbf{y}), \end{aligned} \tag{9}$$

A_d is the drop surface. f_i is the traction on the boundary. We use a proper Green's function that adds a contribution $G_{ij}^{w}(\mathbf{x},\mathbf{y})$ to the free space Green's function $G_{ij}^{FS}(\mathbf{x},\mathbf{y})$, so that $G_{ij}(\mathbf{x},\mathbf{y}) = 0$ on the wall.[69] $M_{ijk}(\mathbf{x},\mathbf{y})$ is the stress due to this Green's function. This special property of Green's function along with the no-slip condition eliminates the surface integral over the wall. Using the second part of the governing Eq. (8) inside the drop phase, we can write a similar equation for the velocity field $\tilde{u}_j$ inside the drop (normal are opposite to the outside field) but evaluating at a point $\mathbf{x}$ outside the drop

$$\begin{aligned} 0 = \frac{1}{8\pi\mu_d} \int_{A_d} \tilde{f}_i(\mathbf{y}) G_{ij}(\mathbf{x},\mathbf{y}) dA(\mathbf{y}) - \frac{1}{8\pi} \int_{A_d} \tilde{u}_i(\mathbf{y}) M_{ijk}(\mathbf{x},\mathbf{y}) n_k(\mathbf{y}) dA(\mathbf{y}) \\ -\frac{1}{8\pi\mu_d} \int_{V_d} \tilde{T}_{ik}^{NN}(\mathbf{y}) G_{ij}(\mathbf{x},\mathbf{y}) dV(\mathbf{y}). \end{aligned} \tag{10}$$

Here V_d is the volume of the drop and $\tilde{f}_i = (\tilde{T}^v_{ij} + \mu_{pd}\tilde{D}_{ij} + \tilde{T}^{NN}_{ij})n_j$ is the total traction at the surface. Note that an integration by parts on the original volume integral term has been performed to convert the divergence term to arrive at (10). From (9) and (10), one obtains

$$u_j(\mathbf{x}) = u_j^\infty - \frac{1}{8\pi\mu_m}\int\limits_{A_d} \Delta f_i(\mathbf{y})G_{ij}(\mathbf{x},\mathbf{y})dA(\mathbf{y}) + \frac{(1-\lambda_\mu)}{8\pi}\int\limits_{A_d} u_i(\mathbf{y})M_{ijk}(\mathbf{x},\mathbf{y})n_k(\mathbf{y})dA(\mathbf{y})$$
$$-\frac{1}{8\pi\mu_m}\int\limits_{V_d}\tilde{T}^{NN}_{ik}(\mathbf{y})G_{ij}(\mathbf{x},\mathbf{y})dV(\mathbf{y}). \tag{11}$$

Here $f_i - \tilde{f}_i \stackrel{\Delta}{=} \Delta f = \Gamma(\nabla\cdot\mathbf{n})\mathbf{n} \quad$ on A^d. In the far-field, we use a one-term Taylor-series expansion around the center of the drop $\mathbf{y}_c$,

$$\begin{aligned} G_{ij}(\mathbf{x},\mathbf{y}) &= G_{ij}(\mathbf{x},\mathbf{y}_c) + \frac{\partial G_{ij}(\mathbf{x},\mathbf{y}_c)}{\partial y_{ck}}(y_k - y_{ck}) + O\left(\frac{a}{|\mathbf{y}-\mathbf{y}_c|}\right)^3, \\ M_{ijk}(\mathbf{x},\mathbf{y}) &= M_{ijk}(\mathbf{x},\mathbf{y}_c) + O\left(\frac{a}{|\mathbf{y}-\mathbf{y}_c|}\right)^3. \end{aligned} \tag{12}$$

For a force-free drop ($\int\limits_{A_d}\Delta f_j(\mathbf{y})dA(\mathbf{y}) = 0$) using incompressibility ($\int\limits_{A_d} u_k(\mathbf{y})n_k(\mathbf{y})dA(\mathbf{y}) = 0$), we obtain

$$\begin{aligned} u_j(\mathbf{x}) &= u_j^\infty(\mathbf{x}) - \frac{1}{8\pi\mu_m}\frac{\partial G_{ij}(\mathbf{x},\mathbf{y}_c)}{\partial y_{ck}} \times \left\{\Gamma\int\limits_{A_d}\left(\frac{\delta_{ik}}{3} - n_i n_k\right)dA(\mathbf{y}) - \mu_m\left(1-\lambda_\mu\right)\right. \\ &\quad \left.\times\int\limits_{A_d}(u_i n_k + u_k n_i)(\mathbf{y})dA(\mathbf{y}) + \int\limits_{V_d} T^{NN\prime}_{ik}(\mathbf{y})dV(\mathbf{y})\right\} \\ &= u_j^\infty(\mathbf{x}) - \frac{1}{8\pi\mu_m}\frac{\partial G_{ij}(\mathbf{x},\mathbf{y}_c)}{\partial y_{ck}}\left(S^{\mathrm{int}\,\prime}_{ik} + S^{vrat\,\prime}_{ik} + S^{NN\,\prime}_{ik}\right) \\ &= u_j^\infty(\mathbf{x}) - \frac{1}{8\pi\mu_m}\frac{\partial G_{ij}(\mathbf{x},\mathbf{y}_c)}{\partial y_{ck}}\left(S^{\mathrm{int}}_{ik} + S^{vrat}_{ik} + S^{NN}_{ik}\right), \end{aligned} \tag{13}$$

where

$$\begin{aligned} S^{\mathrm{int}\prime}_{ik} &= \Gamma\int\left(\frac{\delta_{ik}}{3} - n_i n_k\right)dA(\mathbf{y}), \\ S^{vrat\prime}_{ik} &= -\mu_m\left(1-\lambda_\mu\right)\int\limits_{A_d}(u_i n_k + u_k n_i)(\mathbf{y})dA(\mathbf{y}), \\ S^{NN\prime}_{ik} &= \int\limits_{V_d} T^{NN\prime}_{ik}(\mathbf{y})d \end{aligned} \tag{14}$$

are the contributions to the stresslet due to the interfacial tension, viscosity ratio, and the non-Newtonian effects. These terms without primes in the last expression in (13) represent their traceless forms (due to incompressibility, $\partial G_{ik}(\mathbf{x},\mathbf{y}_c)/\partial y_{ck} = 0$; the trace of the stresslet does not contribute). An identity due to Rosenkilde[70] is used to transform the interfacial part S^{int}_{ik} to the interface tensor $\int(\delta_{ik}/3 - n_i n_k)\,dA(\mathbf{y})$ first so defined by Batchelor.[71]

Using an expression for the image propagator near a rigid wall[12] with normal $\mathbf{n}$, one obtains from (13),

$$u_j^{\mathrm{drift}} n_j = -\frac{1}{8\pi\mu_m}\left(\frac{9}{8h^2}\right)\left(S^{\mathrm{int}}_{ik} + S^{\mathrm{vrat}}_{ik} + S^{NN}_{ik}\right)n_i n_k, \quad \left(\frac{a}{h}\right)^2 \ll 1. \tag{15}$$

For the case here with the wall at $x_2 = y = 0$, the migration velocity is

$$U_{lat} = -\frac{1}{8\pi\mu_m}\left(\frac{9}{8h^2}\right)\left(S_{22}^{\text{int}} + S_{22}^{\text{vrat}} + S_{22}^{NN}\right). \tag{16}$$

Note that the non-Newtonian part S_{22}^{NN} can be shown to be arising from the difference between the first and the second normal stress differences:[46]

$$S_{22}^{NN} = \int\limits_{V_d}\left(T_{22}^{NN'} - \frac{T_{22}^{NN'} + T_{11}^{NN'} + T_{33}^{NN'}}{3}\right)dV = \int\limits_{V_d}\left(\frac{N_1^{NN'} - N_2^{NN'}}{3}\right)dV. \tag{17}$$

In (16), the second term is absent for a viscosity matched system ($\lambda_\mu = 1$). For the N/V case,[46] we showed the theory to be only valid away from the wall. We therefore choose a distance of $h = 2.45a$ where Newtonian comparison works well for examining the effects of the viscoelasticity.

In Fig. 6(a), we plot $-S_{22}^{\text{int}}$, which is the only contribution for a Newtonian system, showing that it varies nonmonotonically with increasing viscoelasticity—first increases and then decreases—similar to the migration velocity. $-S_{22}^{\text{int}}$ is a purely geometric quantity and is determined by the instantaneous drop shape. Increasing deformation and decreasing angle of inclination increase it. We saw in Figure 4 that with increasing *De*, the deformation decreases monotonically but inclination angle shows a

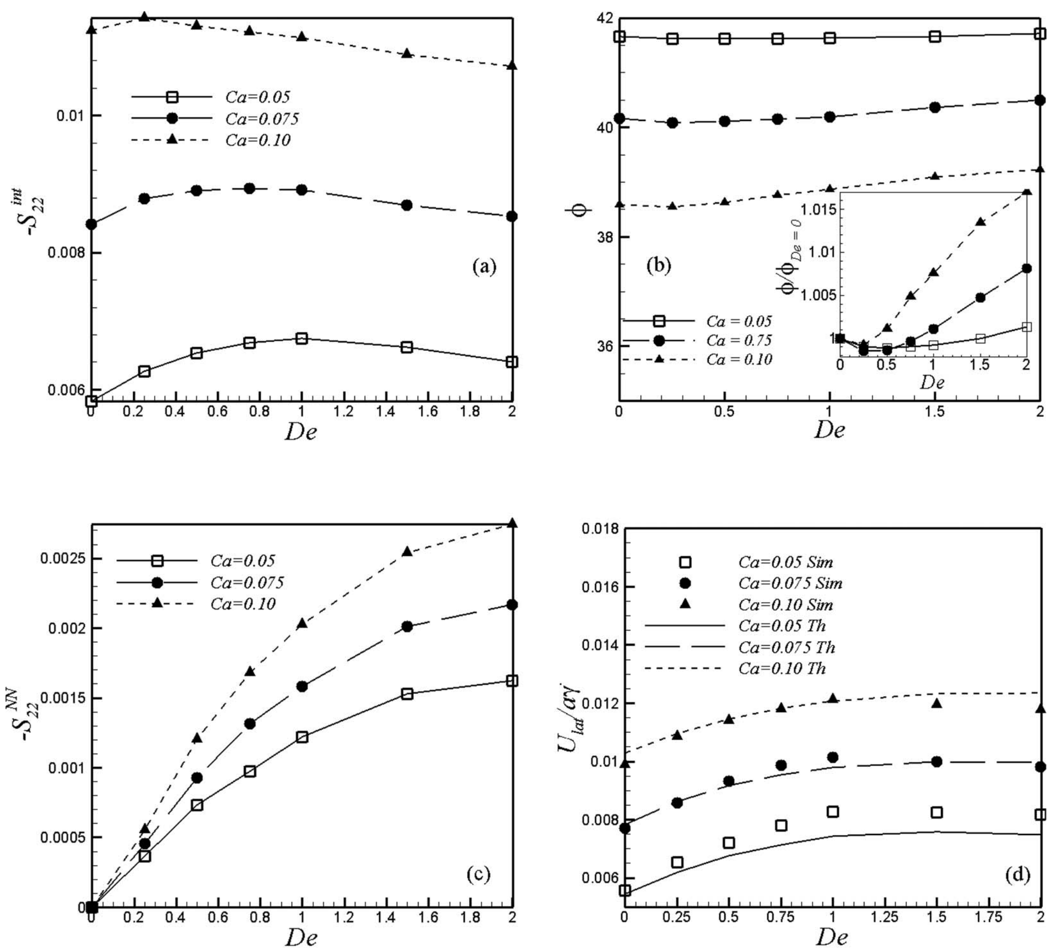

FIG. 6. (a) Interfacial part of the stresslet as a function of *De* for two values of *Ca* at *h/a* = 2.45. (b) Inclination angle for the same cases; inset shows the inclination normalized by its Newtonian value. (c) Non-Newtonian part of the stresslet for the same cases. (d) Migration velocity from the far-field theory (*Th*) is compared with those from the simulations (*Sim*) for varying *De* at three *Ca* values.

nonmonotonic variation with *De* first decreasing and then increasing. Here, we again show the nonmonotonicity of the angle for several Ca values in Fig. 6(b). The non-Newtonian part $-S_{22}^{NN}$ shown in Fig. 6(c) adds a positive contribution to the migration velocity. Note that for the N/V case, $-S_{22}^{NN}$ was negative which thereby retarded migration away from the wall.[46] Finally, in Fig. 6(d), we compare the lateral velocities for viscoelastic cases between the theory and simulations for three values of *Ca*. The theory matches well with the simulation, capturing the nonmonotonic variation, the slight difference arising from the finite Reynolds number (Re = 0.03) of our simulation. In the N/V case investigated previously, the inclination angle decreases with increasing *De*; the geometric stresslet $-S_{22}^{\text{int}}$ due to interfacial tension increases, but the overall velocity variation with *De* is dictated by the non-Newtonian contribution $-S_{22}^{NN}$ that decreases with *De*. Here the nonmonotonic velocity variation with *De* is dictated by the interfacial part $-S_{22}^{\text{int}}$ caused by the variation in the angle of inclination.

C. Effects of viscosity ratio and super-critical *Ca* for breakup

In this section, we very briefly study the effects of viscosity ratio to show how it can significantly affect the dynamics especially for those capillary numbers where viscosity matched system gives rise to large deformation and eventual breakup. In Fig. 7(a), we plot the lateral migration velocities for varying *De* for $Ca = 0.5$ at a high viscosity ratio $\lambda_\mu = 10$. This is above the critical capillary number

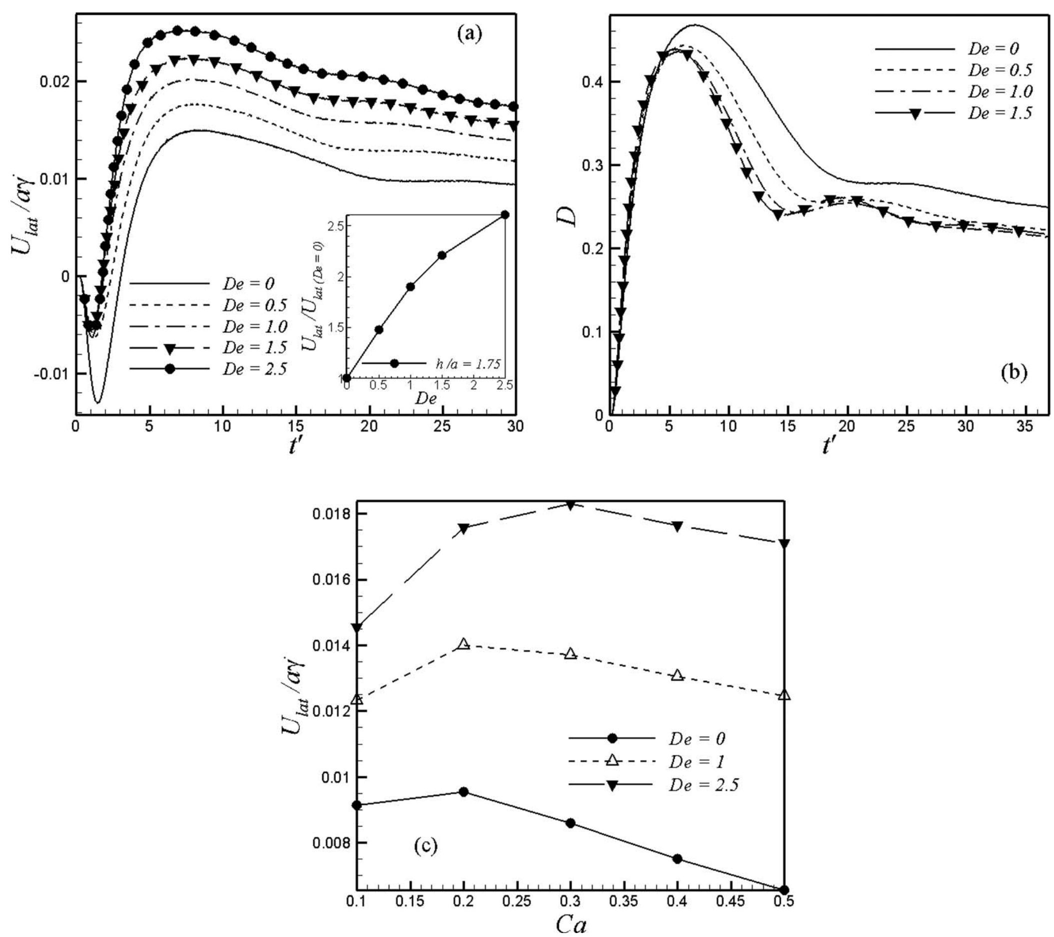

FIG. 7. Evolution of (a) lateral migration and (b) deformation for varying *De* at $Ca = 0.5$ and $\lambda_\mu = 10$. Inset of (a) plots the instantaneous normalized velocity (with respect to the Newtonian value) vs. *De* at $h/a = 1.75$. (c) Migration velocity as a function of *Ca* for different *De* values at $h/a = 1.75$ and $\lambda_\mu = 10$.

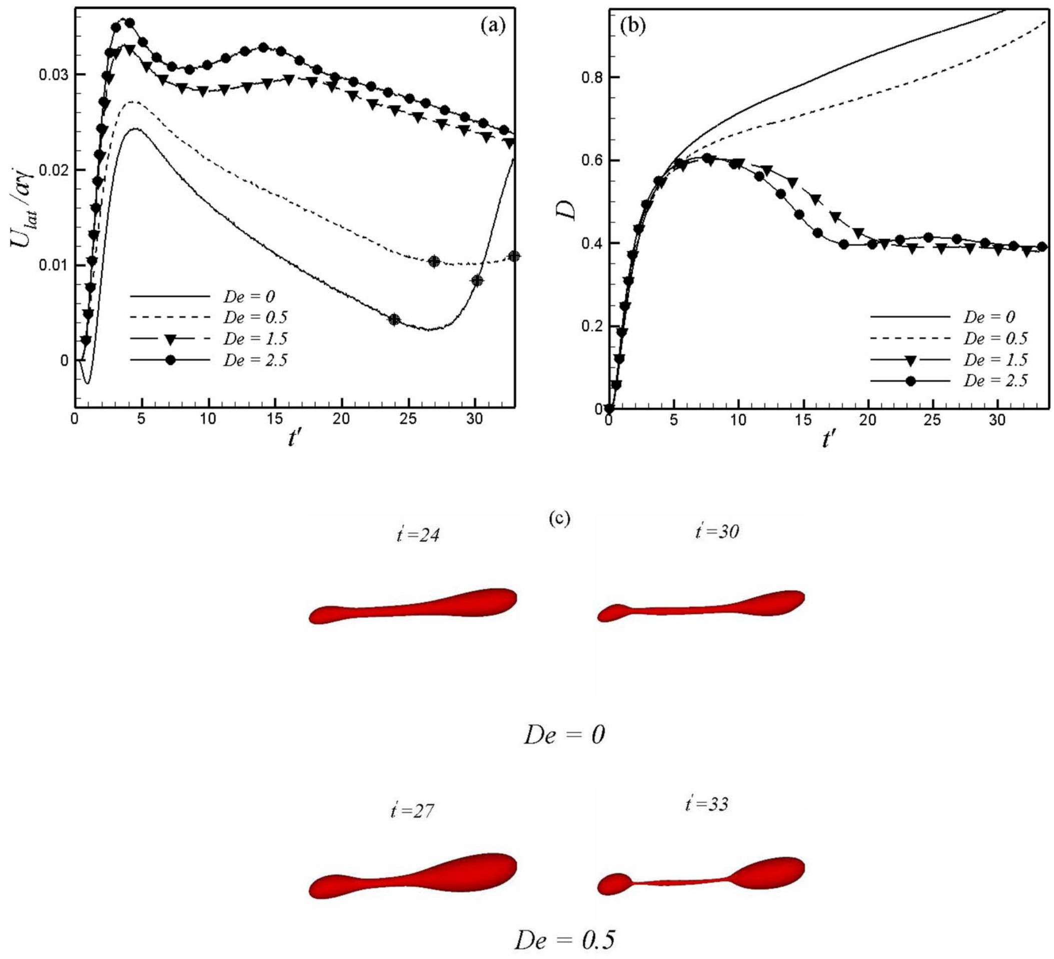

FIG. 8. Evolution of (a) lateral migration, (b) deformation for varying De at $Ca = 0.5$ and $\lambda_\mu = 3.5$. (c) Drop shapes for $De = 0$ and 0.5 before and after the minima; time instants are shown and also marked in part (a).

for breakup for viscosity matched Newtonian system. Yet the drop shapes here remain bounded due to the stabilizing effects of the drop phase viscoelasticity and the higher viscosity ratio. We notice that the migration velocity increases monotonically with De, unlike that of a viscosity matched system where the velocity is non-monotonic (Fig. 2(b)). Inset plots the instantaneous velocities (normalized by the Newtonian value) as a function of De, at $h/a = 1.75$. Also, note that the increase in velocity relative to the Newtonian case is much larger than the viscosity matched system—more than 100% compared to 20% in Fig. 5(a) $\beta = 0.5$ case. The evolution of drop deformation plotted in Fig 7(b) shows that increasing viscoelasticity decreases the initial overshoot in deformation. Fig. 7(c) shows that at this high viscosity ratio of 10, migration velocity varies nonmonotonicaly with Ca for all De values unlike the viscosity matched case. Such non-monotonicity for high viscosity ratio cases was also observed in a Newtonian system.[27]

In Fig. 8(a), we plot the time evolution of the lateral velocity for Newtonian and several Deborah number cases for the same $Ca = 0.5$ and an intermediate viscosity ratio $\lambda_\mu = 3.5$. Corresponding deformation is plotted in Fig. 8(b). At this intermediate viscosity ratio, for the Newtonian case and $De = 0.5$, drops experience breakup, and therefore do not reach a quasi-steady state. On the other hand, higher Deborah number cases $De = 1.5$ and 2.5 result in bounded shapes. For the lower two Deborah cases, the sudden increase in the velocity after reaching a minimum is because of the necking that forms at large deformation. Similar behavior was also observed for N/V systems.[46] In Fig. 8(c) drop shapes are shown for De = 0 and 0.5 before and after the velocity minimum (marked in Fig. 8(a)). After the minimum, the drop shapes are more of two droplets connected by a thread like structure.

V. CONCLUSIONS

The dynamics of a migrating viscoelastic (FENE-MCR) drop in a Newtonian liquid subjected to a wall bounded shear is numerically investigated. Similar to a purely Newtonian system, the drop settles down to a quasi-steady motion where the dynamics is independent of the initial position and the velocity approximately scales with capillary number and the inverse square of the separation from the wall. With increasing Deborah number, the velocity initially increases, but eventually decreases at high values of Deborah or Wisssenberg number. Using a Green's function formulation of the problem, we have developed a far-field analytical expression of the migration velocity. It describes the migration as caused by the stresslet field due to the drop in presence of the wall. The analytical expression contains a distinct component to the stresslet field contributed by the differences between the first and the second normal stress differences inside the drop. The theory matches with the simulated migration velocity capturing the nonmonotonic trend. The nonmonotonicity is caused by the variation in drop inclination angle. Viscoelastic effects on migration are larger at high viscosity ratios; it can prevent drop break up for drops that would break in viscosity-matched system. It can also generate nonmonotonic variation of velocity with capillary number which has also been noticed for Newtonian systems.

ACKNOWLEDGMENTS

K.S. acknowledges partial financial support from NSF Grant Nos. CBET-0625599, CBET-0651912, CBET-1033256, DMR-1239105, CBET-1205322, and NIH Grant No. P20RR016472.

[1] D. J. McClements and J. Weiss, *Bailey's Industrial Oil and Fat Products*, 6th ed. (John Wiley & Sons, Inc., 2005).
[2] S. Friberg, K. Larsson, and J. Sjöblom, *Food Emulsions*, 4th ed. (Dekker, 2007).
[3] J. Kubát and A. Szalánczi, "Polymer-glass separation in the spiral mold test," Polym. Eng. Sci. **14**, 873 (1974).
[4] L. R. Schmidt, "Glass bead-filled polypropylene. Part II. Mold-filling studies during injection molding," Polym. Eng. Sci. **17**, 666 (1977).
[5] G. J. Tangelder, H. C. Teirlinck, D. W. Slaaf, and R. S. Reneman, "Distribution of blood-platelets flowing in arterioles," Am. J. Phys. **248**(3), H318–H323 (1985). Accession number: WOS:A1985ADR5100004.
[6] N. Pamme, "Continuous flow separations in microfluidic devices," Lab Chip **7**, 1644 (2007).
[7] F. P. Bretherton, "The motion of rigid particles in a shear flow at low Reynolds number," J. Fluid Mech. **14**, 284–304 (1962).
[8] L. G. Leal, *Advanced Transport Phenomena: Fluid Mechanics and Convective Transport Processes* (Cambridge University Press, 2007).
[9] P. G. Saffman, "On the motion of small spheroidal particles in a viscous liquid," J. Fluid Mech. **1**, 540–553 (1956).
[10] P. C. H. Chan and L. G. Leal, "An experimental study of drop migration in shear flow between concentric cylinders," Intl. J. Multiphase Flow **7**, 83 (1981).
[11] A. Karnis and S. G. Mason, "Particle motions in sheared suspensions. XXIII. Wall migration of fluid drops," J. Colloid Interface Sci. **24**, 164 (1967).
[12] J. R. Smart and D. T. Leighton, Jr., "Measurement of the drift of a droplet due to the presence of a plane," Phys. Fluids A **3**, 21–28 (1991).
[13] M. R. King and D. T. Leighton, "Measurement of the inertial lift on a moving sphere in contact with a plane wall in a shear flow," Phys. Fluids. **9**, 1248–1255 (1997).
[14] M. R. King and D. T. Leighton, "Measurement of shear-induced dispersion in a dilute emulsion," Phys. Fluids. **13**, 397–406 (2001).
[15] H. L. Goldsmith and S. G. Mason, "The flow of suspensions through tubes. I. Single spheres, rods, and discs," J. Colloid Sci. **17**, 448 (1962).
[16] S. D. Hudson, "Wall migration and shear-induced diffusion of fluid droplets in emulsions," Phys. Fluids **15**, 1106–1113 (2003).
[17] F. Takemura and J. Magnaudet, "Lateral migration of a small spherical buoyant particle in a wall-bounded linear shear flow," Phys. Fluids **21**, 083303 (2009).
[18] C. E. Chaffey, H. Brenner, and S. G. Mason, "Particle motions in sheared suspensions XVIII: Wall migration," Rheol. Acta **4**, 64 (1965).
[19] P. Vasseur and R. G. Cox, "Lateral migration of a spherical-particle in 2-dimensional shear flows," J. Fluid Mech. **78**, 385–413 (1976).
[20] S. Haber and G. Hetsroni, "The dynamics of a deformable drop suspended in an unbounded Stokes flow," J. Fluid Mech. **49**, 257–277 (1971).

[21] P. R. Wohl and S. I. Rubinow, "The transverse force on a drop in an unbounded parabolic flow," J. Fluid Mech. **62**, 185–207 (1974).
[22] M. Shapira and S. Haber, "Low Reynolds number motion of a droplet between two parallel plates," Intl. J. Multiphase Flow **14**, 483 (1988).
[23] M. Shapira and S. Haber, "Low Reynolds number motion of a droplet in shear flow including wall effects," Intl. J. Multiphase Flow **16**, 305 (1990).
[24] T. Imaeda, "Shear-induced migration of a droplet in the presence of a plane wall," Physica A **285**, 306 (2000).
[25] J. S. Halow and G. B. Wills, "Radial migration of spherical particles in Couette systems," AIChE J. **16**, 281 (1970).
[26] J. Magnaudet, S. H. U. Takagi, and D. Legendre, "Drag, deformation and lateral migration of a buoyant drop moving near a wall," J. Fluid Mech. **476**, 115–157 (2003).
[27] W. S. J. Uijttewaal and E. J. Nijhof, "The motion of a droplet subjected to linear shear flow including the presence of a plane wall," J. Fluid Mech. **302**, 45–63 (1995).
[28] W. S. J. Uijttewaal, E. J. Nijhof, and R. M. Heethaar, "Droplet migration, deformation, and orientation in the presence of a plane wall: A numerical study compared with analytical theories," Phys. Fluids A **5**, 819–825 (1993).
[29] M. R. Kennedy, C. Pozrikidis, and R. Skalak, "Motion and deformation of liquid-drops, and the rheology of dilute emulsions in simple shear-flow," Comput. Fluids **23**, 251–278 (1994).
[30] L. G. Leal, "Particle motions in a viscous fluid," Annu. Rev. Fluid Mech. **12**, 435–476 (1980).
[31] H. Brenner, "Hydrodynamic resistance of particles at small Reynolds numbers," edited by J. W. H. Thomas, B. Drew, and V. Theodore, in *Advances in Chemical Engineering*, 6th ed. (Academic Press, 1966), p. 287.
[32] A. Karnis and S. G. Mason, "Particle motions in sheared suspensions. XIX. Viscoelastic media," Trans. Soc. Rheol. **10**, 571–592 (1966).
[33] F. Gauthier, H. L. Goldsmith, and S. G. Mason, "Particle motions in non-Newtonian media I: Couette flow," Rheol. Acta **10**, 344–364 (1971).
[34] E. Bartram, H. L. Goldsmith, and S. G. Mason, "Particle motions in non-Newtonian media III. Further observations in elasticoviscous fluids," Rheol. Acta **14**, 776–782 (1975).
[35] J. Feng and D. D. Joseph, "The motion of solid particles suspended in viscoelastic liquids under torsional shear," J. Fluid Mech. **324**, 199–222 (1996).
[36] B. M. Lormand and R. J. Phillips, "Sphere migration in oscillatory Couette flow of a viscoelastic fluid," J. Rheol. **48**, 551–570 (2004).
[37] T. E. Karis, D. C. Prieve, and S. L. Rosen, "Lateral migration of a rigid sphere in torsional flow of a viscoelastic fluid," AIChE J. **30**, 631 (1984).
[38] T. E. Karis, D. C. Prieve, and S. L. Rosen, "Anomalous lateral migration of a rigid sphere in torsional flow of a viscoelastic fluid," J. Rheol. **28**, 381–392 (1984).
[39] D. C. Prieve, M. S. Jhon, and T. L. Koenig, "Anomalous migration of a rigid sphere in torsional flow of a viscoelastic fluid. II. Effect of shear rate," J. Rheol. **29**, 639–654 (1985).
[40] F. Gauthier, H. L. Goldsmit, and S. G. Mason, "Particle motions in non-Newtonian media. II. Poiseuille flow," Trans. Soc. Rheol. **15**, 297–330 (1971).
[41] G. D'Avino, P. L. Maffettone, F. Greco, and M. A. Hulsen, "Viscoelasticity-induced migration of a rigid sphere in confined shear flow," J. Non-Newtonian Fluid Mech. **165**, 466 (2010).
[42] G. D'Avino, T. Tuccillo, P. L. Maffettone, F. Greco, and M. A. Hulsen, "Numerical simulations of particle migration in a viscoelastic fluid subjected to shear flow," Comput. Fluids. **39**, 709–721 (2010).
[43] G. D'Avino, M. A. Hulsen, F. Greco, and P. L. Maffettone, "Bistability and metabistability scenario in the dynamics of an ellipsoidal particle in a sheared viscoelastic fluid," Phys. Rev. E **89**, 043006 (2014).
[44] R. Pasquino, G. D'Avino, P. L. Maffettone, F. Greco, and N. Grizzuti, "Migration and chaining of noncolloidal spheres suspended in a sheared viscoelastic medium. Experiments and numerical simulations," J. Non-Newtonian Fluid Mech. **203**, 1–8 (2014).
[45] P. C. H. Chan and L. G. Leal, "The motion of a deformable drop in a second-order fluid," J. Fluid Mech. **92**, 131–170 (1979).
[46] S. Mukherjee and K. Sarkar, "Effects of matrix viscoelasticity on the lateral migration of a deformable drop in a wall-bounded shear," J. Fluid Mech. **727**, 318–345 (2013).
[47] S. Caserta, G. D'Avino, F. Greco, S. Guido, and P. L. Maffettone, "Migration of a sphere in a viscoelastic fluid under planar shear flow: Experiments and numerical predictions," Soft Matter **7**, 1100–1106 (2011).
[48] N. Aggarwal and K. Sarkar, "Deformation and breakup of a viscoelastic drop in a Newtonian matrix under steady shear," J. Fluid Mech. **584**, 1–21 (2007).
[49] N. Aggarwal and K. Sarkar, "Effects of matrix viscoelasticity on viscous and viscoelastic drop deformation in a shear flow," J. Fluid Mech. **601**, 63–84 (2008).
[50] N. Aggarwal and K. Sarkar, "Rheology of an emulsion of viscoelastic drops in steady shear," J. Non-Newtonian Fluid Mech. **150**, 19–31 (2008).
[51] S. Mukherjee and K. Sarkar, "Effects of viscosity ratio on deformation of a viscoelastic drop in a Newtonian matrix under steady shear," J. Non-Newtonian Fluid Mech. **160**, 104–112 (2009).
[52] S. Mukherjee and K. Sarkar, "Effects of viscoelasticity on the retraction of a sheared drop," J. Non-Newtonian Fluid Mech. **165**, 340–349 (2010).
[53] K. Sarkar and W. R. Schowalter, "Deformation of a two-dimensional viscoelastic drop at non-zero Reynolds number in time-periodic extensional flows," J. Non-Newtonian Fluid Mech. **95**, 315–342 (2000).
[54] S. Mukherjee and K. Sarkar, "Viscoelastic drop falling through a viscous medium," Phys. Fluids **23**, 013101 (2011).
[55] T. Tavgac, Ph.D thesis, Chemical Engineering, University of Houston, Texas, 1972.
[56] R. W. Flumerfelt, "Drop breakup in simple shear fields of viscoelastic fluids," Indust. Eng. Chem. Fundament. **11**, 312–318 (1972).

[57] P. T. Yue, J. J. Feng, C. Liu, and J. Shen, "Viscoelastic effects on drop deformation in steady shear," J. Fluid Mech. **540**, 427–437 (2005).
[58] G. Tryggvason, B. Bunner, A. Esmaeeli, D. Juric, N. Al-Rawahi, W. Tauber *et al.*, "A front-tracking method for the computations of multiphase flow," J. Comput. Phys. **169**, 708–759 (2001).
[59] M. D. Chilcott and J. M. Rallison, "Creeping flow of dilute polymer solutions past cylinders and spheres," J. Non-Newtonian Fluid Mech. **29**, 381 (1988).
[60] P. J. Coates, R. C. Armstrong, and R. A. Brown, "Calculation of steady-state viscoelastic flow through axisymmetric contractions with the EEME formulation," J. Non-Newtonian Fluid Mech. **42**, 141 (1992).
[61] H. M. Matos, M. A. Alves, and P. J. Oliveira, "New formulation for stress calculation: Application to viscoelastic flow in a T-junction," Num. Heat Transfer. Part B **56**, 351 (2010).
[62] M. Moyers-Gonzalez and I. Frigaard, "The critical wall velocity for stabilization of plane Couetteâ Poiseuille flow of viscoelastic fluids," J. Non-Newtonian Fluid Mech. **165**, 441 (2010).
[63] P. J. Oliveira and A. l. I. P. Miranda, "A numerical study of steady and unsteady viscoelastic flow past bounded cylinders," J. Non-Newtonian Fluid Mech. **127**, 51 (2005).
[64] G. N. Rocha, R. J. Poole, and P. J. Oliveira, "Bifurcation phenomena in viscoelastic flows through a symmetric 1:4 expansion," J. Non-Newtonian Fluid Mech. **141**, 1 (2007).
[65] M. Sahin and R. G. Owens, "On the effects of viscoelasticity on two-dimensional vortex dynamics in the cylinder wake," J. Non-Newtonian Fluid Mech. **123**, 121 (2004).
[66] M. M. Villone, G. D'Avino, M. A. Hulsen, F. Greco, and P. L. Maffettone, "Particle motion in square channel flow of a viscoelastic liquid: Migration vs. secondary flows," J. Non-Newtonian Fluid Mech. **195**, 1–8 (2013).
[67] K. Verhulst, R. Cardinaels, P. Moldenaers, Y. Renardy, and S. Afkhami, "Influence of viscoelasticity on drop deformation and orientation in shear flow Part 1. Stationary states," J. Non-Newtonian Fluid Mech. **156**, 29–43 (2009).
[68] R. K. Singh, X. Y. Li, and K. Sarkar, "Lateral migration of a capsule in plane shear near a wall," J. Fluid Mech. **739**, 421–443 (2014).
[69] J. R. Blake, "Image system for a stokeslet in a no-slip boundary," Proc. Cambridge Philos. Soc.-Math. Phys. Sci. **70**, 303 (1971).
[70] C. E. Rosenkilde, "Surface-energy tensors," J. Math. Phys. **8**, 84–88 (1967).
[71] G. K. Batchelor, "Stress system in a suspension of force-free particles," J. Fluid Mech. **41**, 545–570 (1970).